

Article

In-Line Target Production for Laser IFE

Irina Aleksandrova, Eugeny Koshelev and Elena Koresheva * 

P.N. Lebedev Physical Institute of the Russian Academy of Sciences, 119991 Moscow, Russia;
ivaaleks@gmail.com (I.A.); 2814rosti@mail.ru (E.K.)

* Correspondence: elena.koresheva@gmail.com; Tel.: +7-916-159-3641

Received: 25 December 2019; Accepted: 15 January 2020; Published: 18 January 2020



Featured Application: Fuel target supply to high repetition rate laser facilities including inertial confinement fusion power plant.

Abstract: The paper presents the results of mathematical and experimental modeling of in-line production of inertial fusion energy (IFE) targets of a reactor-scaled design. The technical approach is the free-standing target (FST) layering method in line-moving spherical shells. This includes each step of the fabrication and injection processes in the FST transmission line (FST-TL) considered as a potential solution of the problem of mass target manufacturing. Finally, we discuss the development strategy of the FST-TL creation seeking to develop commercial power production based on laser IFE.

Keywords: inertial fusion energy; free-standing target layering; FST transmission line

1. Introduction

In the frame of International Atomic Energy Agency (IAEA) project (IAEA CRP F13016), one of the specific objectives was to define options for fuel target material choice and mass manufacturing methods, requirements, development pathways and potential solutions [1]. In this paper we identify the principle challenges associated with progression from single shot to high repetition rate operation with regard to manufacturing methods of a cryogenic fuel target (everywhere further—target) for laser IFE.

A fusion power plant will consume as many as one million targets per day. Therefore, the free-standing target transmission line (FST-TL) is an integral part of any IFE reactor. Hereupon, methodologies of the fabrication and injection processes must be applicable to mass-production layering at low cost.

To meet the above requirements, the LPI has proposed to use line-moving and free-standing targets to develop a scientific and technological base for repeatable target supply at the laser focus [2–5]. Precisely moving targets co-operate all production steps in the FST-TL that is considered as a potential solution of mass-production layering and noncontact target delivery in pulsed, repetitively cycled IFE systems. This approach includes also the development of nano-layering technologies, which supports the fuel layer survivability under target injection and transport through the reactor chamber (everywhere further—FST layering method) [6–8].

The target production area includes high-precision technologies for target fabrication, injection and tracking. These technologies are currently an important research stage in the leading laboratories of the world [9–18]. Target compression and ignition is regarded as a major challenge to the IFE community. In addition, to maintain an acceptable tritium inventory, it is needed the development of reasonably fast layering techniques. An overview of various fuel layering methods is given in Reference [2,19].

A traditional approach is based on the following concept: targets for laser experiments are filled by permeation, and a uniform D–T ice layer (molecular composition: 25% of D₂, 50% of DT molecules,

and 25% of T_2) is formed by “beta layering” method [19–21]. This method involves crystallization from a single seed crystal in the fixed target. The process takes place in the anisotropic hydrogen isotopes with extremely slow cooling ($q \sim 3 \cdot 10^{-5}$ K/s) and precise temperature control (<100 μ K) for obtaining cryogenic layers like a single crystal. Long-run beta-layering process at very strict isothermal conditions requires ~ 24 h for one attempt. But routine practice is between 1 and 4 attempts, or even 6 attempts [20,21] which generally require several days or a week. The beta-layering method can form a spherical fuel layer in the uniform thermal environment, but the ability of the D–T targets to withstand acceleration during injection is a key issue in terms of surface perturbation growth in the anisotropic layers under thermal and mechanical loads. Such layers also do not contribute to avoiding the Rayleigh–Taylor instabilities during implosion that decreases the odds for achieving ignition [22]. Moreover, this method is not efficient for repetitively cycled schedule of the target fabrication and injection because the target must be precisely located in the reaction chamber under precise temperature control. We emphasize that even in the single-shot laser experiments an important role for achieving ignition (apart from anisotropic layers) can play some other factors, such as effect of the target support on ice-layer quality, cryogenic shroud retraction, vibration control, target alignment, etc. As noted in Reference [9,13], the beta-layering targets currently cost thousands of dollars apiece; thereby, over the next several years, the focus of the target layering should be on the isotropic fuel structure formation within moving targets to meet the requirements of implosion physics. This places significant onus on the IFE laboratories in the area of new layering methods development.

At the Lebedev Physical Institute (LPI) the researches focus on the extension of the FST layering method (cooling rates $q = 1 - 50$ K/s) on large cryogenic targets to form isotropic ultrafine solid fuel. Our philosophy in conceptualizing the in-line target production is based on the FST layering method to generate a dynamical symmetrization of the liquid fuel within moving targets (instead of solid fuel redistribution inherent in the traditional approach for motionless targets [19]). During FST layering, two processes are mostly responsible for maintaining a fast fuel layer formation (Figure 1):

- Firstly, the target rotation when it rolls down along the layering channel (LC) (n -fold-spirals at $n = 1, 2, 3$) results in a liquid layer symmetrization;
- Secondly, the heat-transport outside the target via the conduction through a small contact area between the shell wall and the LC wall. The spiral LC is a special insert into the cryostat, and it is cooled outside by helium. A contact spot moving along the outer surface of the rotating target results in a liquid layer freezing.

For all these reasons, the FST layering method is a promising candidate for development of the FST-TL at a high repetitively cycled capability intended for mass manufacturing of low cost IFE targets. As a result of long-term research effort, the LPI gained a unique experience in the development of the FST layering module (FST-LM) for target fabrication with an isotropic ultrafine fuel layer inside polymer (CH) shells of 1-to-2-mm diameter. Below, we discuss the FST-LM development of the next-generation for targets over 2 mm in diameter.

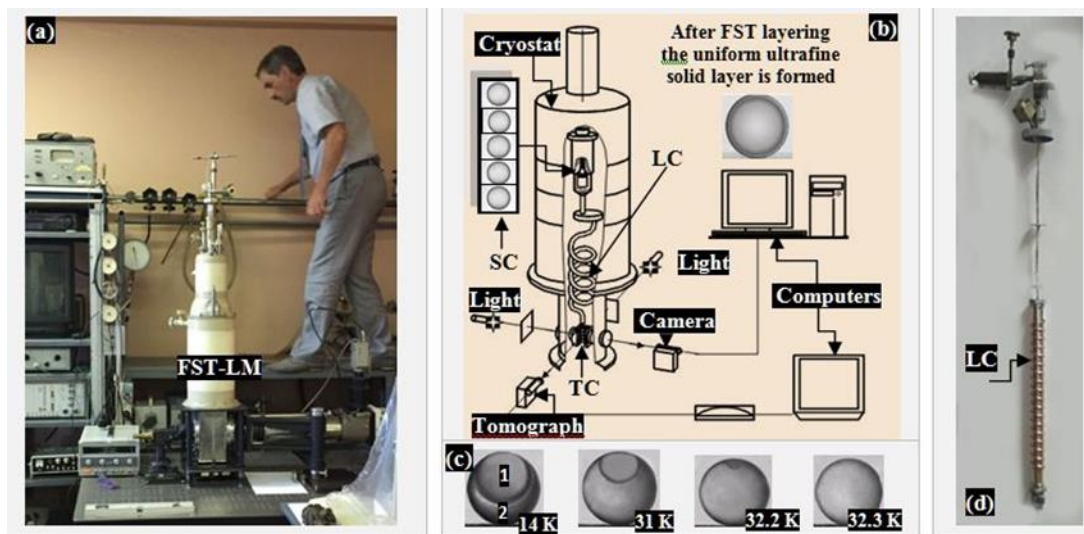


Figure 1. Free-standing target (FST)-layering setup. In (a): general view; in (b): FST-layering module (LM)—target transport is injection between the basic units: shell container (SC)—layering channel (LC)—test chamber (TC)); in (c): (vapor (1) – liquid (2)) interface behavior in 1-mm CH-shell ($P = 765 \text{ atm}$ of H_2 at 300 K); in (d): LC as a part of the insert into the cryostat.

2. Modeling Results

2.1. FST-Layering Method for Classical High Gain Targets

Among the reactor-scale targets is a classical high gain target (CHGT-1) with the following parameters [23]: it is a 4-mm diameter CH shell with a $45\text{-}\mu\text{m}$ thick wall, the cryogenic layer thickness is $200 \mu\text{m}$. For the CHGT-1, in our previous work we calculated the value of τ_{form} for different initial target temperatures T_{in} [6] (Table 1).

Table 1. FST layering time for classical high gain target (CHGT-1).

CHGT-1 Design		τ_{form}	
		$T_{\text{in}} = 37 \text{ K}$	$T_{\text{in}} = 27 \text{ K}$
1	CH shell without overcoat	227.5 c	149.0 c
2	Gold-coated CH shell	13.65 c	8.94 c

Another example of a classical high gain target (CHGT-2) was proposed in Reference [24]. The target consists of four parts: a gold-coated CH shell, a D–T filled CH foam ablator, a layer of pure solid D–T fuel, and a D–T vapor cavity. We use this CHGT-2 to examine issues affecting the possibility of its fabrication by the FST layering method taking into account that it has a very thin CH shell ($1 \mu\text{m}$) compared with CHGT-1 ($45 \mu\text{m}$).

The CHGT-2 specifications are given in Table 2, where D_i and D_0 are the inner and the outer diameters of each layer, and Δ_l and ρ_l are the layer thickness and density, respectively. A thin CH layer has a gold overcoat ($0.03 \mu\text{m}$) to withstand the thermal chamber environment.

Table 2. CHGT-2 specifications.

Material	D _i (μm)	Δ _l (μm)	D ₀ (μm)	ρ _l (g/cm ³)
D–T (vapor)	0	3000	3000	0.3·10 ⁻³
D–T (solid)	3000	190	3380	0.25
CH (DT) ₆₄	3380	261	3902	0.25775
CH layer	3902	1	3904	1.07

The program on CHGT-2 modeling includes the computation of the FST layering time and the LC specifications, such as: number of spirals, inclination angle of the spiral, total length of the spiral, the spiral diameter, and number of turns. The obtained results will allow one to calculate the baseline parameters necessary at designing of the FST-LM as a means of high-gain direct-drive target production.

For a better understanding of the time-integral performance (TIP) criterion under the FST-LM operation, we emphasize that the LC must have a well-defined geometry to satisfy the condition:

$$\text{Target is formed in the LC if } \tau_{\text{form}} \leq \tau_{\text{res}}, \tag{1}$$

where τ_{form} is the layering time, and τ_{res} is the time of target residence in the LC. Since a liquid sagged fuel is the initial state before the FST layering (Figure 1c), then for dynamical fuel symmetrization in a batch of rolling targets the time of liquid phase existence, τ_{liquid} , is a key parameter and must be sufficient for layer symmetrization. This depends on the temperature T_{in} of the target entry into the LC and on the temperature distribution along the LC, i.e., the temperature profiling procedure can play an important role for successful FST layering.

Generally, one can view the target motion in the following rolling conditions:

- Target slides on the LC surface (no rotation: sliding and only sliding or pure S&S-mode);
- Target combines rolling with sliding (rolling with sliding or mixed R&S-mode);
- Target rolls on the LC surface without sliding (rolling and only rolling or pure R&R-mode).

A key problem of our investigations is that it is necessary to realize only the R&R-mode to avoid the outer shell roughening and to achieve the fuel layer uniformity. Therefore, the TIP criterion can be written in the following type (τ_{rol} is the time of pure target rolling):

$$\tau_{\text{form}} \leq \tau_{\text{res}} = \tau_{\text{rol}}. \tag{2}$$

Thus, determination of the rolling conditions is one of the main problem, which influences the choice of the FST-LM operation including simplifying the physics design and modifying the specifications. First of all we should to determine the spiral angles α for realizing the pure target rolling (R&R-mode).

Consider a cylindrical spiral of radius R_0 . In each point of the spiral the tangent makes a constant angle α with the horizontal. Let a spherical target of radius R and mass m is moving with a velocity $V(t)$ along the spiral LC. Then the system of equations in accordance with Newton’s second law of motion has the following form:

$$dV/dt = g\sin\alpha - F_f/m, \tag{3}$$

$$(J/R)d\omega/dt = F_f - k_r, \tag{4}$$

where g is the free fall acceleration, J and ω are the moment of the target inertia and the angular velocity of its rotation, F_f is the friction force, N is the reaction of support from the LC wall, and k_r is the rolling friction. If the target rolls without sliding the linear and angular velocities are related by equation of rolling

$$V = \omega R. \tag{5}$$

Excluding the friction force from Equation (3), we obtain the rolling equation:

$$(1+\zeta)dV/dt = g\sin\alpha - k_r N/m, \zeta = J/(mR^2). \tag{6}$$

Besides, there is the conditional relation that should be maintained for the accelerated target to be in pure rolling:

$$F_f \leq F_{\max} = k_s N, N = m\cos\alpha\{g^2 + (V^4\cos^2\alpha)/R^2\}^{0.5}, \tag{7}$$

where k_s is the sliding friction. The second component under the root is the square of the centripetal acceleration. Solving together Equations (6) and (7), we obtain the working range $\Delta\alpha$, which is given by two inequalities:

$$k_r = \text{tg}\alpha_{\min} < \text{tg}\alpha < \text{tg}\alpha_{\max} = \{(1+\zeta)k_s - k_r\}/\zeta. \tag{8}$$

The next step is modeling of the CHGT-2 layering. We used a simulation code based on solving the Stephen’s problem [25,26]. Using the data in Table 2 and the data on the fuel heat capacity and conductivity [19], we got the following values:

- $T_{\text{in}} = T_s \sim 35 \text{ K}$: $\tau_{\text{form}} = 22.45 \text{ s}$ for D_2 fuel and $\tau_{\text{form}} = 28.52 \text{ s}$ for D–T fuel,
- $T_{\text{in}} = T_d \sim 28 \text{ K}$: $\tau_{\text{form}} = 12.05 \text{ s}$ for D_2 fuel and $\tau_{\text{form}} = 14.25 \text{ s}$ for D–T fuel,

where T_s is the temperature of fuel separation into the liquid and gaseous phases, and T_d is the depressurization temperature at which the excess gas is removed from the SC. Note that depending on the shell strength T_d can be $\sim T_s$.

The final step is the computation a set of the optimization parameters related to the LC geometry to maintain the process of the CHGT-2 fabrication by the FST layering method. Using (8), we have found that the CHGT-2 can be fabricated in the FST-LM by using a double-spiral LC that is confirmed by the experimental modeling with pilot LC mockups. The obtained results are presented below.

1. Double-spiral LC:

- Specifications (baseline design: Spiral 1 + Spiral 2): angle of each spiral – $\alpha = 11.50$, radius of each spiral – 21 mm, height of each spiral – 450 mm, length of each spiral – 2.261 m, total spiral length – 4.52 m, total time of target rolling – 23.49 s;
- $T_{\text{in}} \sim T_d \rightarrow$ the double-spiral LC specifications are those at which the TIP criterion (2) is valid for both D_2 and D–T fuel;
- $T_{\text{in}} \sim T_s \rightarrow$ the TIP criterion is valid for D_2 fuel;
- $T_{\text{in}} \sim T_s \rightarrow$ the TIP criterion is not valid for D–T fuel.

Nevertheless, the double-spiral LC can work in the latter case, as well, because the length of Spiral 2 can be extended on $\sim 2 \text{ m}$ to meet the TIP criterion (Figure 2). Generally, this approach is workable for any spiral LC because several interchangeable spirals with different parameters can be joined to a baseline LC that depends on the experimental goals.

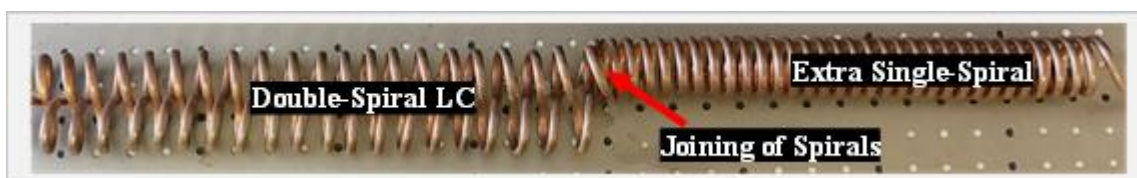


Figure 2. Test mockup of a double-spiral LC with an extra working spiral having a different inclination angle.

For the CHGT-2 we have considered a three-fold-spiral LC, as well. The obtained results are presented below.

2. Tree-fold-spiral LC:

- Specifications #1 (baseline design: Spiral 1 + Spiral 2 + Spiral 3): angle of each spiral – $\alpha = 16.70$, radius of each spiral – 21 mm, height of each spiral – 88 cm, length of each spiral – 3.066 m, total spiral length – 9.187 m, total time of target rolling – 33.29 s;
- Specifications #2 (Specifications #1 + Spiral 4). Spiral 4: angle – $\alpha = 30$, radius – 21 mm, height – 10.8 cm, length – 2.070 m, total length of Spiral 3 and Spiral 4 – 5.136 m. Other words, this 3-fold LC is designed in a special configuration with an extra short Spiral 4 (combined LC).

The modeling has shown that, in ~ 5 s after a start, the target motion is carried out with a constant velocity $V_{\max} = 0.3$ m/s. The total rolling time for Specifications #1 is 33.29 s. Thus, we can realize the rolling conditions for the CHGT-2 and satisfy the TIP criterion in the case of 3-fold-spiral LC, even with a certain time margin.

Note also that the proposed 3-fold-spiral LC (Specifications #1) can have an extra spiral (Specifications #2) so that two spirals “Spiral 3 + Spiral 4” make a combined LC in which the Spiral 4 parameters differ considerably from those of Spiral 3. Such combined LC consists of these spirals assembled one after another: “acceleration Spiral 3 + deceleration Spiral 4” for controlling the target velocity at the output. For example, in our case, it will take no more than 1.5 s at $\alpha = 30$ to zero the target velocity. The obtained results are summarized in Table 3 in which $\tau_{2\text{rol}}$ and $\tau_{3\text{rol}}$ are the rolling times for the double-spiral LC and for the tree-fold-spiral LC, respectively.

Table 3. FST layering for both D_2 and D–T.

D_2 Fuel			
Calculation			Experiment
T_{in}	τ_{form}	$\tau_{2\text{rol}}$	$\tau_{2\text{rol}}$
35.0 K	22.45 s	23.49 s	23.5 s (min)
27.5 K	12.05 s		
D–T Fuel			
Calculation			Experiment
T_{in}	τ_{form}	$\tau_{3\text{rol}}$	$\tau_{3\text{rol}}$
37.5 K	28.52 s	33.29 s	35 s (min)
28.0 K	14.25 s	34.79 s	

A few comments should be made regarding the gold-coated CH shell. In this case for both D_2 and D–T fuel the layering time $\tau_{\text{form}} < 0.5$ s. This means that in order to have a uniform layer, a temperature profiling along the LC becomes a necessary condition for increase in time of τ_{rol} at temperatures more than the triple point one. In this case T_{in} can be ~ 21 K as the hydrogen isotope vapor pressures near the triple point determine the minimum operating pressures (do not exceed 0.2 atm [19]) that allows one to consider an injection filling procedure. Filling of the CH shells with a cryogenic liquid fuel is suitable for the FST layering method because the fuel in the shell directly before the layering has a two-phase state “Liquid + Vapor” (Figure 1c).

Thus, in the IFE, the FST layering is a credible pathway to a reliable, consistent, and economical target supply. Currently, our studies on the creation of FST-LM lie in the field of compatibility of its work with a noncontact method for delivering targets to the reactor.

2.2. Noncontact Accelerating of a Target

Creation of a delivery system based on noncontact positioning and transport of IFE targets represents one of the major tasks in the IFE research program. The purpose is to maintain a fuel layer quality during the target acceleration and injection at the laser focus. The ability of the target to withstand acceleration during its transport and injection is a key issue in the design of the target delivery system. The stringent requirements to the delivery process are as follows [13,27]: targets

should have a temperature of not higher than 18.3 K; the overloads during its acceleration in the injector can be $a = 500\text{--}1000g$ (but there is a desired acceleration limit $a < 500g$ in order to significantly reduce risks of the target damage due to mechanical overloads arising in the process of its acceleration; targets must be accelerated to high injection velocities (200–400 m/s) to withstand the reaction chamber environment. Therefore, the target acceleration is carried out in a special capsule—target carrier or sabot, which transmits a momentum of motion to the target.

The LPI program includes much development work on creation of different designs of the hybrid accelerators for IFE target transport with levitation. One of the main directions is an electromagnetic accelerator (EM-AC) + PMG-System, where PMG is the permanent magnet guideway. The operational principle is based on a quantum levitation of type-II, high temperature superconductors (HTSC) in the magnetic field. The target temperature ($T = 18.3\text{ K}$) excludes the use of type-I superconductors as they have the critical temperature $T_c < 10\text{ K}$, i.e., their heating above 10 K destroys their superconductivity. At the current research stage, the concept development of a hybrid accelerator «EM-AC + PMG» is complete and proof-of-principle experiments in the mutually normal magnetic fields are carried out. The proposed accelerator is a combination of the acceleration system (field coils generating the traveling magnetic waves) and the levitation system (PMG including a magnetic track). The experimental setup is shown in Figure 3. The PMG consists of 6 rectangular permanent magnets, and two in the middle were covered with a ferromagnetic plate. Along the magnetic track (or acceleration length) the magnetic field is constant ($B = 0.33\text{ T}$ onto the permanent magnet surface), which allows the HTSC-Sabot to move with no energy loss. Normal to the acceleration length, the magnet poles are aligned anti-parallel to each other N-S-N (Figure 3a) that produces a considerably strong gradient along the width of the magnetic track. This gradient prevents the motion of the HTSC-Sabots, and they remain located in the transverse direction (Y-axis in the rectangular coordinate system XYZ).

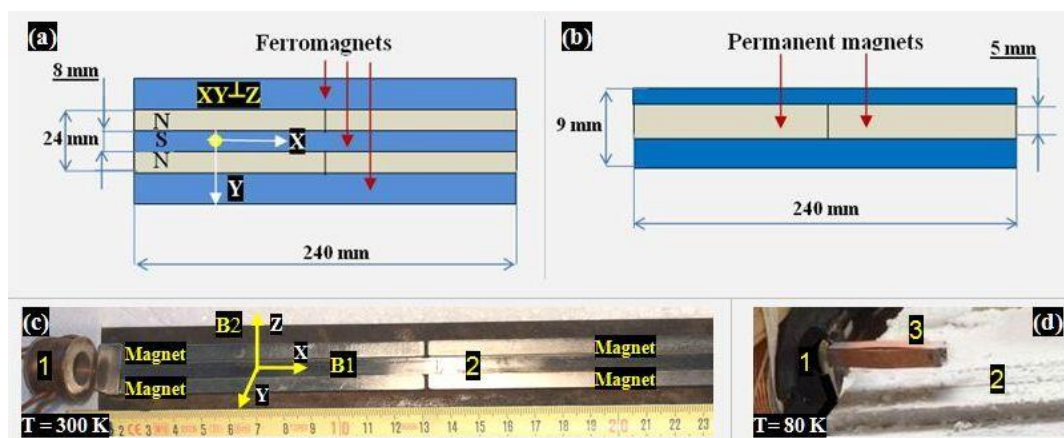


Figure 3. Noncontact acceleration setup. In (a,b): permanent magnet guideway (PMG)-system dimensions (as a whole, it lies on a ferromagnetic substrate); in (c): a top view of the mutual arrangement of the field coil (1) and the PMG-system (2) of two magnets covered with a ferromagnetic plate; in (d): a starting location of the high temperature superconductors (HTSC)-Sabot (3), just before the acceleration, with the directions of the levitation force (vector B_2 in parallel to the Z-axis) and of the driving force (vector B_1 in parallel to the X-axis), as well as along the acceleration length (X-axis).

In our experiments, the HTSC materials are superconducting ceramics based on $\text{YBa}_2\text{Cu}_3\text{O}_{7-x}$ (or Y123) [28] and superconducting tapes of the second generation based on $\text{GdBa}_2\text{Cu}_3\text{O}_{7-x}$ (or Gd123) [29]. These HTSC materials have practically the same values of the critical temperature (T_c) and critical magnetic field (B_c), but they differ from each other in terms of their densities (Table 4) and the magnetic susceptibility (for Y123 ($|\chi| = 2.5 \cdot 10^{-3}$) [28] and for Gd123 ($|\chi| = 4.5 \cdot 10^{-4}$) [29]). Recall that the phenomenon of superconductivity exists only below the values of B_c and T_c [30].

Table 4. Parameters of the HTSC-materials [28,29].

HTSC Type	Density (g/cm ³)	B _c at 0 K (T)	T _c (K)
Y123	$\rho = 4.33$	>45 T	91
Gd123	$\rho = 3.25$	>45 T	92

The experimental setup (Figure 3) operates based on the following effects: the levitation of the HTSC-Sabot is due to the Meissner effect, and the stability of levitation over the PMG system is ensured by vortex pinning [30]. The experiments were made in the mutually normal magnetic fields: the first is **B**₁ (from the field coil to move the HTSC-Sabot) directed along the acceleration length, and the second is **B**₂ (from the permanent magnets to counteract the gravity) directed normally to the acceleration length (Figure 3c). The PMG-system was optimized in order to achieve simultaneously large levitation forces and stability of the levitation after small perturbations (Figure 3a–c). Figure 3d shows a starting location of the HTSC-Sabot (3) just before the acceleration.

A key feature of the proposed PMG-system is that it has a simple arrangement. It is assembled from several individual magnets that allows it to be extended to any required acceleration length and create multi-stage accelerators. We start with a simple case. Figure 4 demonstrates the work of a one-stage accelerator.

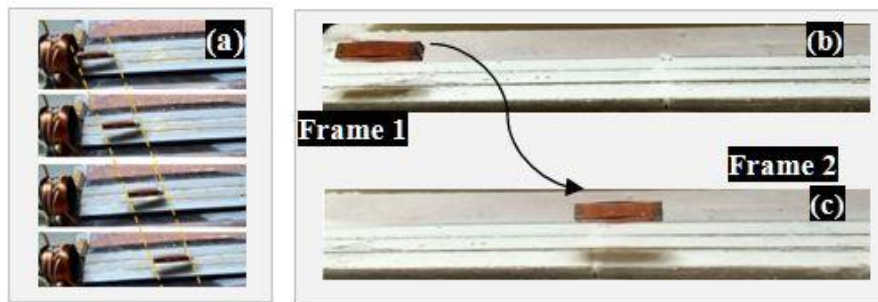


Figure 4. One-stage accelerator: magnetic acceleration of the levitating HTSC-Sabot from Gd123. In (a): results of proof-of-principle (POP) experiments: HTSC-sabot (≤ 30 mm) levitates over the linear PMG-system (~ 30 cm); in (b,c): the HTSC-Sabot looks like it is attached to a magnetic track.

The HTSC-Sabot obtains a velocity of 1 m/s (Figure 4a) and keeps it over the whole acceleration length (22.5 cm, see Figure 3c). The vertical and horizontal levitating drift is not observed (Figure 4b,4c). The levitation height is ~ 3 mm. A set of control experiments has shown that the HTSCs can be successfully used to maintain a friction-free motion of the HTSC-Sabot over the PMG. Besides, they can provide a required stability of the levitation height over the whole acceleration length due to a flux pinning effect [30] inherent in the interaction between a Type-II superconductor and a permanent magnet.

Technologically, the obtained results allow a convenient spacing of the multiple coils (also called a multiple-stages accelerator) and lead to realizing very high velocities of the HTSC-Sabot. In Reference [5], we have reported that, using the MgB₂-superconducting coils [31] as a driving body, it is possible to achieve the required velocity $V_{inj} = 200$ m/s without exceeding the acceleration limits ($a = 400g < 500g$), as well as the injector requirement of ~ 5 m in length. It operates at a very low temperature (~ 18 K) allowing no heat energy to be passed into the target from the accelerating medium. For future IFE power plants, the injection velocities of $V_{inj} > 200$ m/s can be easily achieved because the combination of “EM-AC + PMG-System” successfully works as a multiple-stages accelerator.

Therefore, our next step is the development of a multiple-stages accelerator. Below we propose a first version of such accelerator (Figure 5). Superconducting sabot includes several HTSC components (Figure 5a). It comprises not only the accelerating HTSC-coils but also the HTSC-plates for providing its stable levitation along the magnetic track (Figure 5b). During acceleration, the diameter of the

barrel exceeds the diameter of the HTSC-Sabot (Figure 5c), allowing it to protect the target against the thermal damage and to reduce the risks from wedging of the sabot in the injector guiding tube.

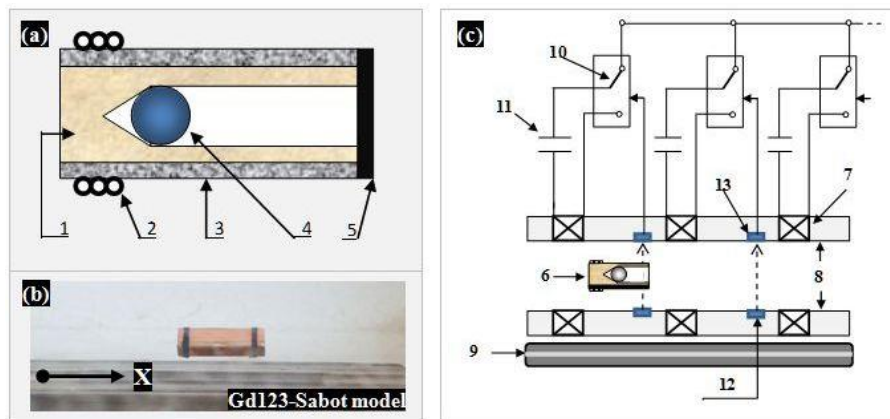


Figure 5. Multiple-stages accelerator for noncontact target transport: (a): HTSC-Sabot, which includes 1—polymer matrix, 2—HTSC-coils (MgB_2 -driving body), 3—HTSC-plates, 4—target, 5—shield or cover to protect the injected target from a head wind of a residual gas in the reaction chamber; (b): levitation of an HTSC-Sabot mockup (made from the Gd123-tapes) over the linear PMG-system at 80 K (magnetic field is equal to 0.33 T on the permanent magnet surface); (c): schematic of the multiple-stages accelerator, which includes 6—HTSC-Sabot, 7—coil, 8—guiding bore, 9—magnetic track, 10—key to run a traveling magnetic wave, 11—capacitor, 12, 13—optocoupler.

Note also that the sequence of field coils loaded on the corresponding capacitance is a line with lumped parameters. From the point of view of the relative position of the accelerating traveling pulse and magnetic dipole (in our case HTSC-Sabot), steady is only the case when an impulse pushes (rather than pulls) a magnetic dipole. This means that the phase (longitudinal) stability is on the front slope of the traveling impulse. Such a technique is called the principle of auto phasing [32] and corresponds to the case of using superconducting materials in the manufacture of the target carriers as they HTSC-Sabot are pushed out from the area of a stronger magnetic field [30].

3. FST-TL Key Elements and Their Functional Description

The free-standing targets are an indispensable requirement for any IFE power plant for continuous target layering and their repeatable injection to the reaction chamber. In other words, targets must remain un-mounted in each production step, and in the IFE experiments, they will be fed directly from the FST-LM to the assembly module with HTSC-Sabots.

3.1. FST Layering Module

Our previous results, as well as the expert analysis carried out in the frame of IAEA CRP 13016 (under the IAEA contract No. 20344 [27]), have shown that the proposed FST-LM (see Figure 1) can meet the requirements for CHGT-2 fabrication.

The construction of the FST-LM is shown in Figure 6.

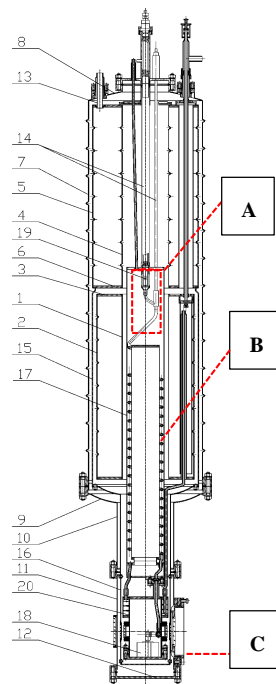


Figure 6. The FST-LM construction: (A) Protection-sluice module, which serves to accommodate the shell container (SC); (B) Layering channel (LC); (C) Test chamber (TC). 1—cryostat housing, 2—nitrogen vessel, 3—thermal shield, 4—helium vessel, 5—well, 6—internal cavities of the insert, 7—liquid-nitrogen transmission line, 8—PSM, 9—place of the SC disposal in PSM, 10—LC, 11—target collector, 12—insert into the helium cryostat well, 13—cryostat neck, 14—traction valve, 15—He-gas output, 16—heat exchanger, and 17—tube space.

The protective-sluice module (Figure 6, item A) serves to accommodate the SC. The LC is made in the form of a tubular spiral (Figure 6, item B), and the outer surface of which is carefully polished and covered with a multilayer screen made of a mylar film to further reduce a degree of the surface blackness.

3.2. FST-Projectile Assembly Module

Before the acceleration and injection stages, the free-standing targets must be mounted in a special module in the form “HTSC-Sabot + Target + Cover” (everywhere further—FST-Projectile). Each step of the assembly process will be operated at significant rates. Several remarks should be made here. In the FST-Projectile, the HTSC-Sabot plays a major role allowing for: (a) to transmit effectively an acceleration pulse to the target, and (b) to protect the target from damage during the acceleration process. An important characteristic of its design is the shape of a target nest. Our study has shown that the shape of the target nest allows one to significantly increase the upper limit of the allowable mechanical overloads on the target and to minimize the injector dimensions. In optimal case the sabot nest should have a conical shape with the angle of 87° [4]. A chart of the HTSC-Sabot with the target placed in the conical nest and the cover is shown in Figure 5a.

The FST-projectile assembly module is shown in Figure 7.

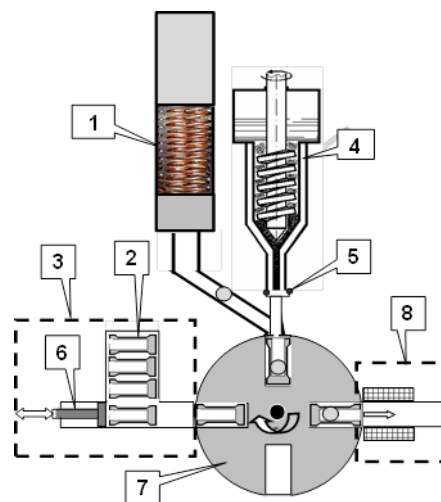


Figure 7. Repeatable assembly of the FST-projectile for safe noncontact delivery of the free-standing targets at the laser focus: 1—FST-LM including a double-spiral LC; 7—target accumulator and system for target transport under gravity to the rotating drum; 3—HTSC-Sabot feeder; 2—a set of the HTSC-Sabots; 3—HTSC-Sabot feeder; 4—extruder of solid D2 cylinder (protective cover production); 5—heater to cut the cover from D2 cylinder; 6—electromagnetic pusher; 7—rotating drum; 8—field coil for the FST-projectile transport to the starting point of the acceleration system.

3.3. Noncontact Delivery System

Our near-term goal is to reduce the acceleration length (~ 5 m) of the linear accelerator by using a circular PMG of 0.5 m in outer diameter (OD) in the HTSC magnetic levitation (maglev) transport system. This HTSC-maglev is intended for the high target velocity applications, target trajectory correction, and creation of a precise injector.

First, experiments with an acceleration length ~ 31.5 cm (corresponding to one full turn of a median circle) were made to demonstrate this approach on laboratory scale tests. Figure 8 shows the process of HTSC-Sabot moving at $T = 80$ K over the circular PMG-system under an electromagnetic driving pulse. The HTSC-Sabot is the same as in the experiments with the linear accelerator (Figure 5b). It is a hollow parallelepiped with dimensions: width 4 mm, height 4 mm, and length 24 mm, which made from the Gd123-tapes with a thickness of 0.3 mm. The HTSC-Sabot mass is 0.2 g. The PMG-system is a neodymium magnet with OD = 10 cm and thickness 5 mm. The internal diameter (ID) is 5 cm. This disc magnet is placed in a ferromagnetic housing open from above (housing thickness 1 mm). Such a configuration allows achieving the desired magnetic field profile over the PMG-system (Figure 8a).



Figure 8. Laboratory scale tests with the PMG-system of a circular type (a–f—consecutive video frames of the HTSC-Sabot counterclock-wise moving).

3.4. Physical Layout of the FST-TL

Currently, the main problems for target fabrication and injection are as follows:

- There are considered various target designs for direct drive IFE (e.g., compare CHGT-1 and CHGT-2);
- For each target design, low cost methods of high rate target fabrication are needed;
- Targets must survive mechanical and thermal loads during injection;
- Noncontact options for target acceleration and repeatable injection are also needed.

A schematic of the FST-TL of repeatable operation satisfying the listed above requirements is shown in Figure 9.

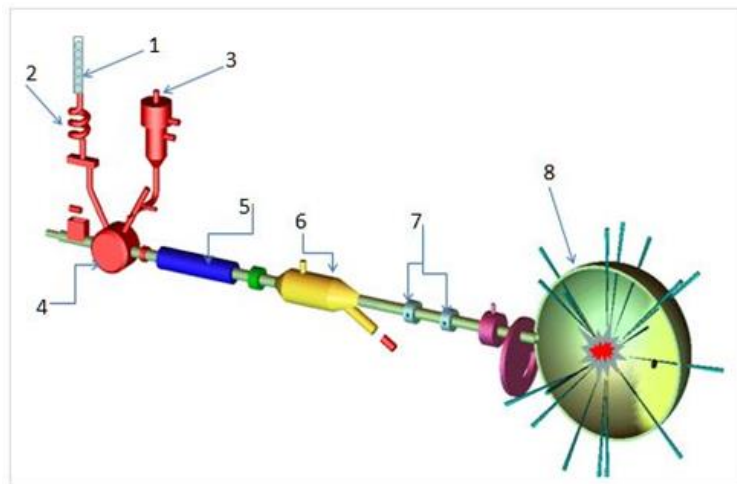


Figure 9. Schematic of the FST- transmission line (TL) operation: 1—SC, 2—FST-LM, 3—extruder for protective cover preparation, 4—FST-Projectile assembly module, 5—noncontact accelerator, 6—FST-Projectile separation module, 7—system for on-line target tracking and characterization, and 8—reaction chamber wall

Note that a scenario of the FST-TL operation in a batch mode has been shown on a reduced scale for the targets under 2 mm in diameter:

- Fuel filling of a batch of 5-to-25 free-standing targets at one time ($P_{\max} = 1000$ atm at 300 K) (Figure 1c);
- Fuel layering within the free-standing and line-moving targets using a single LC (Figure 1d), and the cryogenic layer thickness was up to 100 μm (Figure 1b);
- Levitating HTSC-Sabot acceleration in the mutually normal magnetic fields (Figures 4 and 5b);
- Target injection into the test chamber at a rate of 0.1 Hz at 300 K (Figure 10) and at $T = 4.2$ K (Figure 11a);
- Target tracking and characterization using the Fourier holography methods.

The last point is not a topic of this report. Therefore we only note the results that are important for a general understanding of the problem of techniques integration into a target production line capable of producing the required amount of the cryogenic targets. As shown in Reference [3], the Fourier holography of the image recognition is a promising way for on-line characterization and tracking of the flying targets. In such a scheme the recognition signal is maximal in case of an exact match between the real and the etalon images; the operation rate is several μs . Achievements in the Fourier target characterization embodied in creation of a simulation code developed as special software “HOLOGRAM”. A set of computer experiments have shown that this approach allows to achieve a high accuracy of 0.7 μm in the following operations: (1) recognition of the target imperfections in

both low- & high- harmonics, (2) quality control of both a single target and a target batch, and (3) simultaneous control of the injected target quality, its velocity and trajectory.

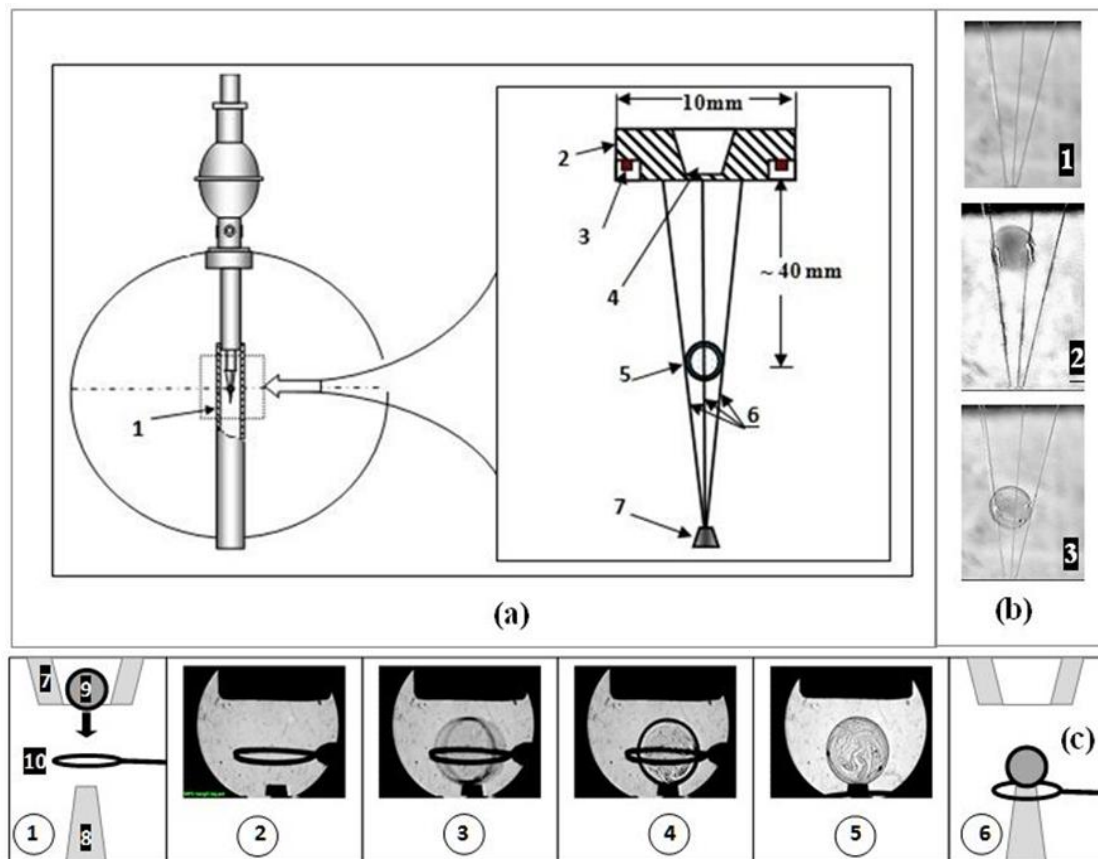


Figure 10. On-holder injection experiments at 300 K (1-6 is the sequence of video frames of the experiment): (a) free target positioning onto the TC bottom; (b) target injection to a special cylindrical cavity imitating a hohlraum-like unit; (c) target injection to a circular PMG-holder.

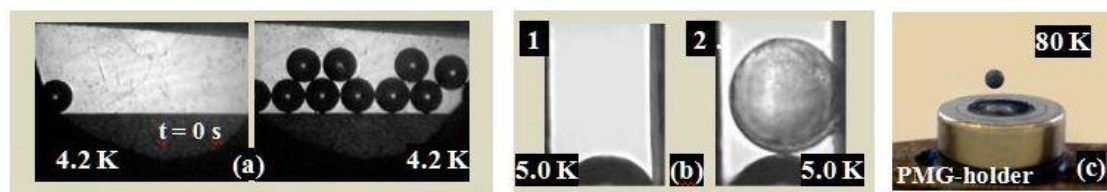


Figure 11. (a–c): A set of the injection experiments at cryogenic temperatures.

4. FST-TL in the Single-Shot Laser Experiments

The FST-TL system shown in Figure 9 can also be used in the laser experiments on a single-shot target irradiation. In this case, it is necessary to capture the injected target on a holder precisely located in advance at the given point. We conducted a series of experiments on the target injection using some different holders: tripod-holder, vacuum suspension on a glass capillary, hohlraum-like unit, and PMG-holder.

In our experiments we have used the gravity injector mounted at the end of the FST-LM. This injector covers a fairly small solid angle (about 15°) which is no greater than the solid angle of any diagnostic means in the reaction chamber. The target transport by injection is an excellent springboard for overcoming a departure between two concepts: mounted and free-standing targets. Figure 10a shows the relative position of the “injector—holder” couple for a multi-beam laser facility, as well as the results of experimental modeling of the free-standing target assembly with the tripod-holder

prearranged at a given point of the test chamber. A final adjustment of the target position relative to the position of the laser focus is carried out using piezoelectric sensors mounted in the tripod base. In Figure 10a, the following designations are accepted: 1—is the retractable cryogenic shroud which must be removed just before the moment of the target irradiation by a laser, 2—output flange; 3—piezoelectric supports made of quartz; 4—nozzle for the target injection from the FST-LM; 5—shell with fuel layer; 6—threads forming a tripod; 7—thread tensioner. The tripod-holder does not require the use of glue for mounting the target, which increases the reliability of operation at cryogenic temperatures and provides a minimum contact area between the target and the threads. The alignment accuracy is $+20\ \mu\text{m}$. The principle of the target alignment is based on the inverse piezoelectric effect which realized by using three rectangular micro-supports made of quartz piezoelectric elements located as shown in Figure 10a (item 3). At the output flange Figure 10a (item 2) there are electrical contacts (not shown in the figure) through which a signal is applied to change the dimensions of these piezoelectric elements. They are small in size and able to work at cryogenic temperatures with a minimal heat loss. The target characterization is based on a backlight shadowgraphy which is a widely used imaging technique. It can provide high contrast object images for a better understanding of an object's shape or size [33]. Specialized software is developed to automatically determine the coordinates of the target and generate commands for correcting its position in real time. Figure 10b shows the details of the injection process on the tripod-holder (1, 2, 3 are the frames before, during, and after the shell injection). The experimental conditions are as follows: CH shell of 2 mm in diameter, the chamber wall temperature is $T = 300\ \text{K}$, the pressure inside it is 1 Torr, the holder is the tripod made from three glass fibers (10 μm in diameter). Figure 10c shows the injection of a 300- μm diameter glass shell under gravity from the nozzle of the FST-LM onto the top of a 90- μm diameter capillary prearranged at a given point of the test chamber (here, the target is trapped by the vacuum mount mechanism using this capillary): 1—schematic of the start shell position, 2–5—step-by-step experiment with target injection and its trapping on the top of the capillary, 6—schematic of the final shell position, 7—nozzle, 8—capillary, 9—shell, and 10—restrictive ring used to reliably position the target on the capillary (this ring is removed from the target irradiation area before the laser shot).

Some other options for the target injection and positioning are shown in Figure 11. A unique feature of these experiments is the target injection at cryogenic temperatures. Experimentally, injection can be carrying out in various ways: (1) directly to the TC with a free target positioning onto the TC bottom (Figure 11a), (2) to a special cylindrical cavity imitating a hohlraum-like unit (Figure 11b), and (3) to a circular PMG-holder, which is a promising way for non-contact manipulation and positioning of the cryogenic targets (Figure 11c). In the latter case, for an active target guidance we used an Y123-coated CH shell of 2 mm in diameter (Y123-layer thickness $\sim 10\ \mu\text{m}$) and a disc magnet with OD = 15 mm, ID = 6 mm, and thickness 5 mm. A ferromagnetic insert is located in the central hole of the magnet. The magnetic field on the periphery of the disc magnet is about 0.3 T.

In the IFE research, these results attract a significant interest due to their potentials for development of the HTSC-maglev suspension technologies and can be used for enhancement of the operating efficiency of the injection process in the single-shot laser experiments.

5. Conclusions

In the direct-drive approach to IFE, the free-standing cryogenic targets of high gain design are required for fueling a laser energy plant. The targets must be delivered to the chamber center with a high accuracy and a high repetition rate. Because fusion reactions must occur approximately ten times per second, the FST-TL becomes an integral part of any fusion reactor. The FST-TL consists of a target production facility, target acceleration, and injection and tracking systems. Currently, target production is in transition from one-of-a-kind to one million of high quality ignition targets per day. Creation of the target delivery system based on noncontact positioning and transport of the cryogenic targets represents one of the major tasks, as well. Therefore, in the frame of IAEA CRP F13016 [1,27], of

particular concern is development of a conceptual design of FST-TL including a mass-manufacturing of reactor-scaled targets and their noncontact delivery at the laser focus.

Achieving controlled thermonuclear ignition is one of the goals for IFE, and a target with the isotropic fuel structure is a critical aspect of successfully reaching that goal. This indicates that currently target fabrication technologies for IFE laser experiments are a challenge. A promising candidate is the FST layering method—fast fuel layering inside moving free-standing targets—which is well suited to economical mass production of IFE targets. The cost of the targets produced by the FST layering method may be several orders of magnitude lower than for the traditional target fabrication capabilities and technologies.

In this paper, high-gain direct-drive cryogenic targets using foam to support the D–T fuel were analyzed. These are the shells of ~4 mm in diameter with a wall from compact and porous polymers. The layer thickness is ~200 μm for pure solid fuel and ~250 μm for in-foam solid fuel. A credible path to solve the issue is the FST layering method developed at the LPI. This method is unique and has no analogs in the world. The computation showed that the layering time for such targets was $\tau_{\text{form}} < 23$ s for D_2 and $\tau_{\text{form}} < 30$ s for D–T fuel, and they can be successfully fabricated by the FST-layering method inside the n -fold LCs at $n = 2, 3$. So, fast fuel layering is a necessary condition for the producing targets in the massive numbers and for obtaining fuel as isotropic ultrafine layers. Namely, isotropic fuel structure supports the layer quality survivability under the target acceleration, injection, and transport through the reactor chamber. For on-line characterization and tracking of the injected targets it is planned to apply the method of coherent optics based on the Fourier holography.

Additionally, throughout this paper, the principle of innovative HTSC-maglev transport systems are explored for the safe, stable and noncontact target delivery at the laser focus. We address this question both by experimentally demonstrating such system performance and by calculating their parameters. The HTSC levitation is based on the interaction between the magnet and the HTSC. Due to unique characteristics, the HTSC materials have demonstrated tremendous potential for the noncontact target transport.

Any maglev scheme has to address three basic properties: levitation, guidance, and acceleration. The characteristics of the permanent magnets composing the guideway in the PMG-system are very important in terms of levitation force and stability. We found that not always complicated magnet arrangements bring significant improvements with respect to some simpler arrangements that also provide large levitation force. In our study we use two simple magnet arrangements: linear and circular. In the experiments with one-stage linear accelerator, the HTSC-Sabot from the second generation tapes Gd123 gains a speed up to ~1 m/s which remains the same over a 22.5-cm magnetic track (movement time is 0.22 s). The calculations have shown that, using the driving body from MgB_2 superconducting cables as an HTSC-Sabot component, allows reaching the injection velocities of 200 m/s at 5-m-acceleration length without exceeding the established restrictions related to the target acceleration ($a = 400 \text{ g} < 500 \text{ g}$). These velocities can be obtained by using a set of the field coils the number of which is more than 100 pieces (multiple-stages accelerator). Besides, our experiments with strongly pinned superconductors (HTSC-sabot) and permanent magnets in the PMG-system display high stability of the levitation and acceleration processes. This is directly related to the safe operation and design of the whole delivery system.

Recent results obtained at the LPI may help improving the actual design of HTSC-maglev accelerators. Significant reduction of the accelerator dimensions and the number of the field coils can be obtained in a circular accelerator, in which only several field coils are arranged in a circle in the PMG-system. In such geometry, the HTSC-sabot will move along a practically constant circular orbit in pulsed, repetitively cycled mode and will gradually gain the required velocity. The LPI is currently making major efforts to create such accelerator to reach the injection velocities in the range of 200–400 m/s with a constant PMG dimension and a constant number of the field coils. This is a novel way to enhance the performance of target accelerators through HTSC guiding technology.

Thus, a unique scientific, engineering and technological base developed at the LPI allows creating a FST-TL prototype for mass targets production with the ultrafine fuel structure and their noncontact delivery at the laser focus. Such targets for application to high repetition rate laser facilities allow one to test the reactor-scaled technologies and to run a pioneering research of laser direct drive using, for the first time, the isotropic hydrogen fuel in the target compression experiments, including a possibility to apply the FST-TL for single-shot laser experiments for achieving the laboratory-based ignition.

Author Contributions: Conceptualization, I.A. and E.K. (Elena Koresheva); software, I.A.; investigation, E.K. (Eugeniy Koshelev) and E.K. (Elena Koresheva); writing—original draft preparation, I.A.; writing—review and editing, E.K. (Elena Koresheva); project administration, E.K. (Elena Koresheva). All authors have read and agreed to the published version of the manuscript.

Funding: This research was funded by the International Atomic Energy Agency (<https://www.iaea.org>) under Research Contract No. 20344 and by the Russian Government in the frame of the State Task Program.

Conflicts of Interest: The authors declare no conflict of interest.

References

1. Pathways to Energy from Inertial Fusion: Materials beyond Ignition. In Proceedings of the 3rd IAEA Research Coordination Meeting of the Coordinated Research Project (F13016), Vienna, Austria, 21–23 January 2019; Available online: <https://www.iaea.org/events/evt1805417> (accessed on 23 January 2019).
2. Aleksandrova, I.; Koresheva, E. Review on high repetition rate and mass production of the cryogenic targets for laser IFE. *High Power Laser Sci. Eng.* **2017**, *5*, e11. [[CrossRef](#)]
3. Aleksandrova, I.; Koresheva, E.; Koshelev, E.; Krokhin, O.; Nikitenko, A.; Osipov, I. Cryogenic hydrogen fuel for controlled inertial confinement fusion (concept of cryogenic target factory based on FST-layering method). *Phys. At. Nucl.* **2017**, *80*, 1227–1248. [[CrossRef](#)]
4. Aleksandrova, I.; Koresheva, E.; Koshelev, E. Multiple target protection methods for target delivery at the focus of high repetition rate laser facilities. *Probl. At. Sci. Technol. Ser. Thermonucl. Fusion* **2018**, *41*, 73–85.
5. Aleksandrova, I.; Akunets, A.; Koresheva, E.; Koshelev, E. Contactless HTSC sabot acceleration by mutually normal magnetic fields generated in a PMG system with magnetic travelling wave. In Proceedings of the XLV International Conference on Plasma Physics and Controlled Thermonuclear Fusion, Moscow, Russia, 2–5 April 2018.
6. Aleksandrova, I.; Koresheva, E.; Osipov, I.; Timasheva, T.; Tolokonnikov, S.; Panina, L.; Belolipetskiy, A.; Yaguzinskiy, L. Ultrafine fuel layers for application to ICF/IFE targets. *Fusion Sci. Technol.* **2013**, *63*, 106–119. [[CrossRef](#)]
7. Aleksandrova, I.; Bazdenkov, S.; Chtcherbakov, V. Rapid fuel layering inside moving free-standing ICF targets: Physical model and simulation code development. *Laser Part. Beams* **2002**, *20*, 13–21. [[CrossRef](#)]
8. Aleksandrova, I.; Bazdenkov, S.; Chtcherbakov, V.; Gromov, A.; Koresheva, E.; Koshelev, E.; Osipov, I.; Yaguzinskiy, L. An efficient method of fuel ice formation in moving free standing ICF/IFE targets. *J. Phys. D Appl. Phys.* **2004**, *37*, 1163–1179. [[CrossRef](#)]
9. Goodin, D.; Aleksander, N.B.; Brown, L.C.; Frey, D.; Gallix, R.; Gibson, C.R.; Maxwell, J.L.; Nobile, A.J.; Olson, C.L.; Petzoldt, R.W.; et al. A cost-effective target supply for inertial fusion energy. *Nucl. Fusion* **2004**, *44*, S254–S265. [[CrossRef](#)]
10. Canaud, B.; Fortin, X.; Garaude, F.; Meyer, C.; Philippe, F. Progress in direct-drive fusion studies for the Laser Mégajoule. *Laser Part. Beams* **2004**, *22*, 109–114. [[CrossRef](#)]
11. Frey, D.; Alexander, N.; Bozek, A.; Goodin, D.; Stemke, R.; Drake, T.; Bitner, D. Mass production methods for fabrication of inertial fusion targets. *Fusion Sci. Technol.* **2007**, *51*, 786–790. [[CrossRef](#)]
12. Bousquet, J.; Hung, J.; Goodin, D.; Alexander, N. Advancement in glow discharge polymer coatings for mass production. *Fusion Sci. Technol.* **2009**, *55*, 446–449. [[CrossRef](#)]
13. National Research Council of the National Academies. Inertial Fusion Energy Technologies. In *An Assessment of the Prospects for Inertial Fusion Energy*; The National Academies Press: Washington, DC, USA, 2013; Chapter 3; pp. 89–105. ISBN 978-0-309-27081-6.

14. Mori, Y.; Nishimura, Y.; Ishii, K.; Hanayama, R.; Kitagawa, Y.; Sekine, T.; Takeuchi, Y.; Satoh, N.; Kurita, T.; Kato, Y.; et al. 1-Hz Bead-Pellet Injection System for Fusion Reaction Engaged by a Laser HAMA Using Ultra-Intense Counter Beams. *Fusion Sci. Technol.* **2019**, *75*, 36–48. [[CrossRef](#)]
15. Mori, Y.; Iwamoto, A.; Ishii, K.; Hanayama, R.; Okihara, S.; Kitagawa, Y.; Nishimura, Y.; Komeda, O.; Hioki, T.; Motohiro, T.; et al. Spherical shell pellet injection system for repetitive laser engagement. *Nucl. Fusion* **2019**, *59*, 096022. [[CrossRef](#)]
16. Ren, L.; Shao, P.; Zhao, D.; Zhou, Y.; Cai, Z.; Hua, N.; Jiao, Z.; Xia, L.; Qiao, Z.; Wu, R.; et al. Target Alignment in the Shen-Guang II Upgrade Laser Facility. *High Power Laser Sci. Eng.* **2018**, *6*, e10. [[CrossRef](#)]
17. Tsuji, R. Trajectory adjusting system using a magnetic lens for a Pb-coated superconducting IFE target. *Fusion Eng. Des.* **2006**, *81*, 2877–2885. [[CrossRef](#)]
18. Kubo, T.; Karino, T.; Kato, H.; Kawata, S. Fuel Pellet Alignment in Heavy-Ion Inertial Fusion Reactor. *IEEE Trans. Plasma Sci.* **2019**, *47*, 2–8. [[CrossRef](#)]
19. Kucheyev, S.O.; Hamza, A.V. Condensed hydrogen for thermonuclear fusion. *J. Appl. Phys.* **2010**, *108*, 091101. [[CrossRef](#)]
20. Koziolowski, B.J.; Mapoles, E.R.; Sater, J.D.; Chernov, A.A.; Moody, J.D.; Lugten, J.B.; Johnson, M.A. Deuterium-Tritium Fuel Layer Formation for the National Ignition Facility. *Fusion Sci. Technol.* **2011**, *59*, 14–25. [[CrossRef](#)]
21. Mapoles, E. Production of hydrogen ice layers for NIF targets. In Proceedings of the 7th International Conference on Inertial Fusion Science and Applications, Bordeaux, France, 12–16 September 2011.
22. Bringa, E.M.; Caro, A.; Victoria, M.; Park, N. Atomistic modeling of wave propagation in nanocrystals. *J. Miner. Met. Mater. Soc.* **2005**, *57*, 67–70. [[CrossRef](#)]
23. Nakai, S.; Miley, G. *Physics of High Power Laser and Matter Interactions*; World Scientific Publishing: Singapore, 1992; Volume 1, pp. 87–90.
24. Bodner, S.; Colombant, D.; Schmitt, A.; Gardner, J.; Lehmborg, R.; Obenschain, S. High Gain Target Design for Laser Fusion. *Phys. Plasmas* **2000**, *7*, 2298–2301. [[CrossRef](#)]
25. Tikhonov, A.N.; Samarsky, A.A. *Equations of Mathematical Physics*; Nauka: Moscow, Russia, 1977.
26. Samarsky, A.A.; Mikhailov, A.P. *Mathematical Modeling: Ideas, Methods, Examples*; Nauka: Moscow, Russia, 2002.
27. Koresheva, E. FST transmission line for mass manufacturing of IFE targets. In Proceedings of the 1st IAEA RCM of the CRP Pathways to Energy from Inertial Fusion: Materials beyond Ignition, Vienna, Austria, 16–19 February 2011; IAEA: Vienna, Austria, 2016.
28. Golovashkin, A.I.; Ivanenko, O.M.; Leitus, G.I.; Mitsen, K.V.; Karpinskii, O.G.; Shamrai, V.F. Anomalous behavior of the structural parameters of the ceramic YBa₂Cu₃O₇ near the superconducting transition. *J. Exp. Theor. Phys. (JETP) Lett.* **1987**, *46*, 410–412.
29. Lee, S.; Petrykin, V.; Molodyk, A.; Samoilenkov, S.; Kaul, A.; Vavilov, A.; Vysotsky, V.; Fetisov, S. Development and production of second generation high T_c superconducting tapes at SuperOx and first tests of model cables. *Supercond. Sci. Technol.* **2014**, *27*, 044022. [[CrossRef](#)]
30. Landau, L.; Lifshitz, E. *Theoretical Physics. Electrodynamics of Continuous Media*, 2nd ed.; Nauka: Moscow, Russia, 1982.
31. Goldacker, W.; Schlachter, S.; Zimmer, S.; Reineret, H. High transport currents in mechanically reinforced MgB₂ wires. *Supercond. Sci. Technol.* **2001**, *14*, 783–786. [[CrossRef](#)]
32. Dolya, S. Acceleration of magnetic dipoles by a sequence of current-carrying turns. *Tech. Phys.* **2014**, *59*, 1694–1697. [[CrossRef](#)]
33. Settles, G.; Hargather, M. A review of recent developments in schlieren and shadowgraph techniques. *Meas. Sci. Technol.* **2017**, *28*, 042001. [[CrossRef](#)]

